Solar Cycle Progression Updated Prediction (Experimental): Validation Document

MARK MIESCH

CIRES/University of Colorado, NOAA Space Weather Prediction Center

Last updated: January 18, 2024

In October 2023, NOAA/SWPC released an experimental solar cycle prediction product on the Space Weather Prediction Testbed (SWPT) website. This product will be updated monthly to provide an accurate, up-to-date prediction for the progression of Solar Cycle 25, which began in 2019 and is expected to peak in 2024. This document provides a technical description of the new product within the context of the pre-existing NOAA/SWPC solar cycle progression product. Furthermore, it describes in detail the procedure that was used to validate the new product before its public release, as required by the NOAA/SWPC Research to Operations (R2O) Pipeline.

1. PRODUCT DESCRIPTION

The events and hazards that the discipline of space weather is concerned with generally originate with magnetic activity on the Sun. The release of magnetic energy powers solar storms such as flares and coronal mass ejections that pose risks to power grids, satellites, telecommunications, airline travel, GPS navigation, and human spaceflight, along with other economic sectors that rely on these technologies (for example finance and precision farming). The frequency and severity of solar storms is in turn regulated by the solar cycle, a quasi-periodic waxing and waning of solar activity that occurs on a time scale of approximately 11 years.

No two solar cycles are the same. They vary in amplitude and duration. Stronger cycles produce more solar storms and pose a larger hazard to our technological society. Forecasting the progression of the solar cycle over the coming months, years, and even decades is therefore of considerable interest to SWPC customers. A notable example is the satellite industry, where launches and mission operations must be planned years in advance.

The most well-known way to track the progression of each solar cycle and quantify its amplitude is to monitor the average number of sunspots visible (with telescopes) on the solar surface over the course of each month. This is commonly referred to as the Sunspot Number, or SSN. This metric has the advantage of a long history; humanity has been regularly monitoring sunspots for over four centuries. Numbered solar cycles begin in the mid-18th century, with the quality and frequency of observations increasing substantially since the early 19th century. We are currently in Solar Cycle 25, which began in December 2019. Solar Cycle 24 reached maximum in April 2014.

Another way to monitor the progression of the Solar Cycle is through the flux of radio waves in the 10.7 cm (2800 MHz) band. Though these radio measurements do not share the 400-year history of sunspot observations, the F10.7 radio flux is found to be highly correlated with solar activity and is less subjective than the quantification of sunspots. NOAA/SWPC currently distributes monthly observations and predictions of the sunspot number and F10.7 radio flux on two public-facing web pages:

<div align="center">

solar-cycle-progression
predicted-sunspot-number-and-radio-flux

</div>

The predicted-sunspot-number-and-radio-flux product is presented in tabular form on the website but it is also distributed as a json (javascript object notation) file:

<div align="center">

predicted-solar-cycle.json

</div>

Since the 1970's, NOAA/SWPC has collaborated with NASA and the International Space Environment Services (ISES) to forecast the amplitude and timing of upcoming solar cycles. NOAA/NASA/ISES panels have been convened to announce formal predictions for Cycle 22 (1989/1990), Cycle 23 (1995), Cycle 24 (2007), and Cycle 25 (2019). These international panels arrive at their prediction by soliciting and synthesizing dozens of distinct predictions from the international solar physics community.

The web-based products referred to above currently highlight the 2019 panel prediction for sunspot number and F10.7 radio flux. However, within a few years, it became clear that this prediction was too low. This is demonstrated in Figure 1, which is taken from SWPC's current solar cycle progression website. The black line shows monthly sunspot observations and the blue line is a 13-month average of these monthly observations. Both curves lie significantly above the 2019 NOAA/NASA/ISES prediction, indicated by the red line with associated uncertainties (shaded region).

ISES Solar Cycle Sunspot Number Progression
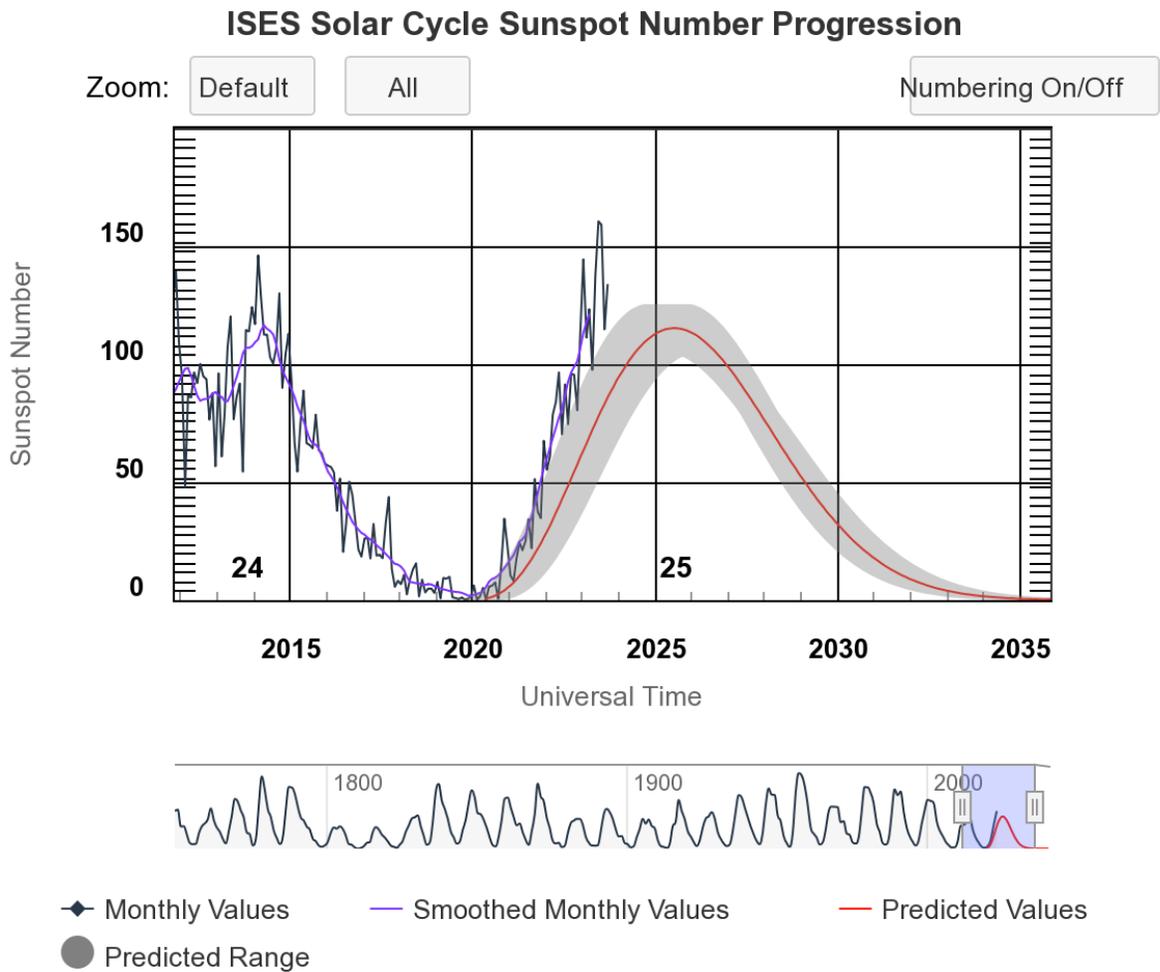
Fig. 1. The solar cycle progression product currently provided on the NOAA/SWPC website, as it appeared in October, 2023. Curves show both sunspot observations (black, blue) and predictions (red, grey), as indicated in the legend. The graphic is interactive, allowing users to select the time interval and information that is displayed.

Though there is some academic interest in following how the 2019 prediction continues to fare, SWPC customers require a more accurate forecast for Impact-based Decision Support Services (IDSS). The 2019 NOAA/NASA/ISES panel made no provision for updating the forecast.

In October 2023, NOAA/SWPC released an experimental solar cycle prediction product on the Space Weather Prediction Testbed (SWPT) website.

The new product, as it appears in October 2023, is shown in Figure 2. It provides an updated forecast for Solar Cycle 25 (magenta, with associated uncertainties) that is expected to be much more accurate than the 2019 NOAA/NASA/ISES panel prediction (red shaded region) for forecasting solar activity through the next decade. Unlike the 2019 prediction, the new experimental product will be continuously updated on a monthly basis as new sunspot and F10.7 observations become available.
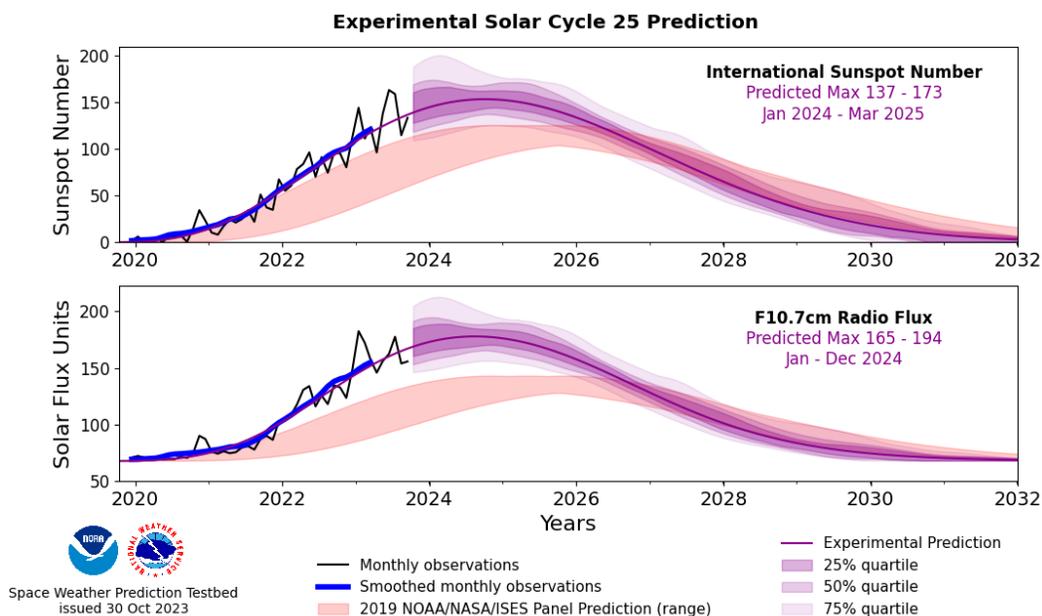
Fig. 2. The (experimental) updated solar cycle prediction product that was released publicly on the Space Weather Prediction Testbed in October, 2023. As indicated in the legend, this displays a new prediction, updated every month, together with the observations and the 2019 panel prediction. Predictions are displayed both for the International Sunspot Number (top) and the F10.7 cm radio flux (bottom).

As in the current product, monthly sunspot observations are obtained from the official maintainer of the International Sunspot Number, which is the World Data Center Sunspot Index and Long-Term Solar Observations (WDC-SILSO) program hosted by the Solar Influences Data Center (SIDC) at the Royal Observatory of Belgium. The monthly F10.7 cm radio flux observations are provided by the Dominion Radio Astrophysical Observatory in Penticton, British Columbia, Canada, which is operated by Natural Resources Canada (NRCan).

The predictions are made by fitting available observations to a nonlinear function that is designed and calibrated to capture the essential features of previous solar cycles (Section 2). An average is then computed between the current fit and one made without the most recent nine months of data. This makes the prediction more robust to short-term trends.

The fitting function for the sunspot number is the same as the function used for the 2019 NOAA/NASA/ISES panel prediction. So the form of the curve has not changed: its parameters have merely been recalibrated to better match observed data.

The approach is similar for the F10.7 prediction. The 2019 panel computed their F10.7 prediction by applying an empirical polynomial conversion to the sunspot number curve. However, we find that fitting the monthly F10.7 observational data directly gives a more accurate prediction than applying a conversion to the sunspot number prediction. The fitting function used for F10.7 makes use of an improved empirical calibration that was not available in 2019. Uncertainties are computed by applying the same prediction procedure to previous solar cycles, at the same point in each cycle (see Sections 2 and 3).

In Figure 2, the uncertainties (quartiles) are only shown for future dates, in this case beyond October, 2023. However, the mean prediction is shown for the full time interval in order to help the reader judge the fidelity of the fit.

In addition to the graphical display in Figure 2, the new product also includes an update predicted-solar-cycle.json file, which can replace the current json file of the same name as well as the tabular display on the predicted-sunspot-

number-and-radio-flux website. The contents of this json file are displayed graphically in Figure 3 for a prediction made in October, 2023.
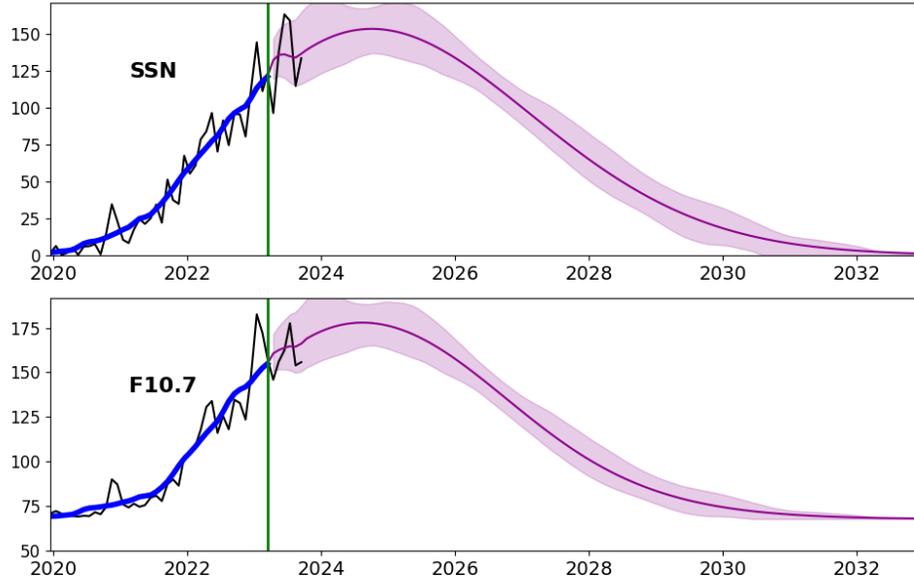
Fig. 3. The contents of the predicted-solar-cycle.json file in the new experimental product. As in Fig. 2, the upper and lower frames show the SSN and F10.7 radio flux predictions (magenta lines), the monthly observations (black lines), and a 13-month boxcar smoothing function applied to the monthly observations (bold blue lines). However, the prediction here is somewhat different than that shown in Fig. 2, incorporating observed monthly values in the transition period just to the right of the vertical green line as described in the text.

As in the current product, the contents of the json file begin 6 months prior to the current date. We refer to the current date as t_p; i.e. the month that the prediction is made. For the result shown in Figure 3, t_p is equal to October, 2023 and the start date of the prediction is April, 2023. This start date for the prediction is indicated in the Figure by the vertical green line.

In order to compute the centered 13-month average for a given date, indicated by the solid blue line, monthly SSN data is needed for 6 months prior and 6 months after that date. So, there is a period of 6 months where monthly SSN data is available but smoothed SSN data is not. We refer to this as the transition period for reasons that will become clear in the next paragraph. So, the transition period begins where the smoothed observations end (vertical green line) and extends to the current date (i.e. the time where the monthly observations end).

For the 6 months that lie within the transition period, some monthly observations are available but not enough to compute a 13-month average. So, we proceed by concatenating the monthly observations for $t < t_p$ to the mean prediction for $t \geq t_p$. Then, to obtain predicted values for the 6 months in the transition period, we apply a 13-month boxcar smoothing function to this composite curve.

So, for $t \geq t_p$, the prediction in the json file (Fig. 3) is identical to that shown by the magenta curves in Figure 2, for both SSN and F10.7. However, within the transition period (which begins 6 months prior to the current date), the predictions contained in the json file include a correction based on the monthly observations in that time period. This improves accuracy for the prediction curve and eases the transition between the smoothed observations and the future prediction.

The shaded area in Figure 3 is computed by adding the median (50% quartile) residual to the prediction curve. Checks are included to ensure that the minimum SSN does not drop below zero and the minimum F10.7 value does not drop below the minimum value, represented by the constant term in equation (4).

2. TECHNICAL DESCRIPTION

Based on close scrutiny of historical sunspot data, Hathaway et al. [4] proposed the following nonlinear function to represent the average shape of the solar cycle, expressed in terms of the sunspot number f as a function of time t:

$$f(t) = \frac{A(t - t_0)^3}{\exp\left[(t - t_0)^2/b^2\right] - c} \tag{1}$$

This function has four parameters. The parameter A largely determines the amplitude of the cycle, though the maximum value also depends weakly on b and c. The curve can be shifted in time by adjusting the parameter t_0, which need not be equal to the accepted cycle start date (it typically falls about 4 months ahead of the official start date). Solar cycles are known to be asymmetric, with relatively fast rise times (4-5 years from min to max), followed by a more gradual decay (6-7 years). This asymmetry is captured by the parameters b (linked to the rise time) and c (linked to the skewness of the decay).

Though observational data can in principle be used to fit all four parameters, this is not optimal for predictive purposes. For example, the skewness of a particular cycle is rarely apparent in the first few years. Furthermore, the parameters are not independent: cycles with larger amplitudes are known to rise faster. Hathaway et al. found that the following relationships captured this behavior well:

$$b = 15.6 + 8.18A^{-1/4} \tag{2}$$

$$c = 0.42 \tag{3}$$

Note that the numerical values of these coefficients are different than those suggested by Hathaway et al. in 1994 [4]. This is because, in the last decade, a substantial international effort was completed to recalibrate the historical sunspot record [1, 2]. This culminated with a major revision of the International Sunspot Number that was released in 2015, now known as Version 2. All reported observations in this document (e.g. Figures 1 and 2) follow the standard set by Version 2 of the International Sunspot Number. The coefficients presented in equations (2) and (3) were recalibrated by D. Hathaway for the NOAA/NASA/ISES Panel in 2019 in order to be consistent with Version 2 of the international SSN.

We find that optimal prediction can be achieved by using these relationships for b and c while applying a two-parameter nonlinear curve fit to the observed monthly sunspot number to obtain A and t_0. The 2019 NOAA/NASA/ISES prediction panel used the same function, with the same parameterizations for b and c. The values of A and t_0 they used were based on their assessment of the cycle predictions solicited from the community. So, the updated prediction (experimental product) only differs in the values of A and t_0, which are calibrated to match the latest observations.

A similar prediction approach based on a two-parameter curve fit (A, t_0) has been recently employed by Upton & Hathaway [9]. However, they used different parameterizations for b and c. We considered these updated parameterizations but found that they performed no better than those used by the 2019 panel (Section 3). With little evidence for a significant improvement in accuracy, we chose to retain the original 2019 panel formulation in order to keep as much consistency with the existing product as possible.

A potential problem with this prediction approach is that it can occasionally be susceptible to abrupt changes in slope in the early years of a cycle. This is most dramatically illustrated when applying the prediction method to Cycle 24, as shown in Figure 4.

Here the dotted black line represents the observed monthly sunspot data and the smoothed observational data (bold black line) is only plotted up to the prediction date, taken to be 3, 5, 7, and 9 years into the cycle as indicated. The blue line and shaded region indicate the mean prediction with uncertainty, as in Figure 2. The red lines indicate the maximum residual over all viable cycles (uncertainties and residuals are further explained later in this section).

The main point of Figure 4 is to highlight the prediction made three years into the cycle (upper left), which proves to be much too high because it is determined primarily by a sharp rise in activity around 2011. In order to provide a more robust result, we average the prediction at a given time with the prediction made nine months prior. This is demonstrated in Figure 5, which is to be compared with Figure 4.

The averaging of two lead times mitigates the over-prediction in year 3 without significantly changing the prediction in years 5, 7, and 9. Experimentation revealed a difference of 9 months to be the optimal interval between the two lead times to improve robustness without sacrificing accuracy (Section 3).

Thus far in this Section we have explained how the mean sunspot number prediction (solid magenta line) in Figure 2 has been computed. We now describe how the uncertainties (magenta shaded regions) are computed. Figure 5 serves as a useful reference for how this is done.

The smoothed observations (bold solid black line) are only shown up to the prediction time but they can be computed independent of prediction time for the full range of the cycle because we have the data (black dotted line). So, for any prediction time of any past cycle, we can compute the difference between the mean prediction (magenta line) and the smoothed observations (bold solid black line) for the entire range of the cycle. We refer to this as the **residual**. So the residual is a function of three variables: the time t (relative to cycle beginning), the prediction time t_p, and the cycle number n.

We can in principle compute the residual for all past cycles for which there is data, namely Cycles 1 through 24. However, the sparsity of observations for the first 5 cycles precludes a reliable determination of the cycle amplitude and
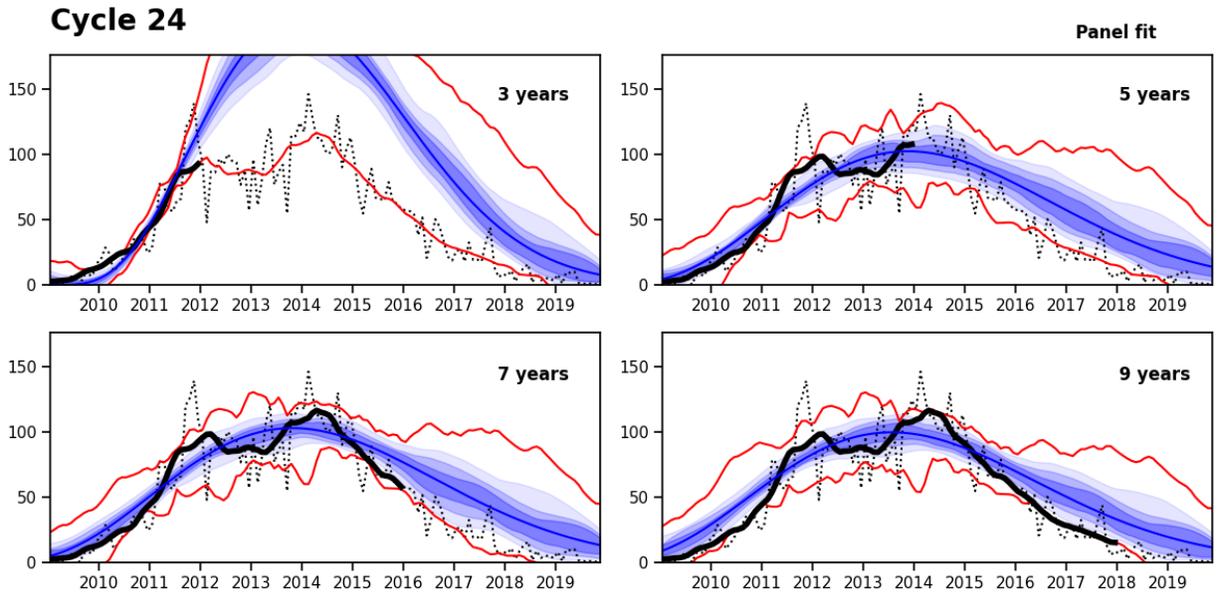
Fig. 4. The dotted black line in each frame shows the observed monthly sunspot number (SSN) for Cycle 24. The blue line shows the prediction made 3, 5, 7, and 9 years into the cycle by means of a two-parameter curve fit to eqn. (1) as described in the text. Shaded regions show the smoothed 25, 50, and 75 percent quartiles as in Fig. 2. Red lines indicate the unsmoothed 100% quartiles. The 13-month average of the observed monthly SSN is shown as a solid black line, but is only displayed up to the prediction time.
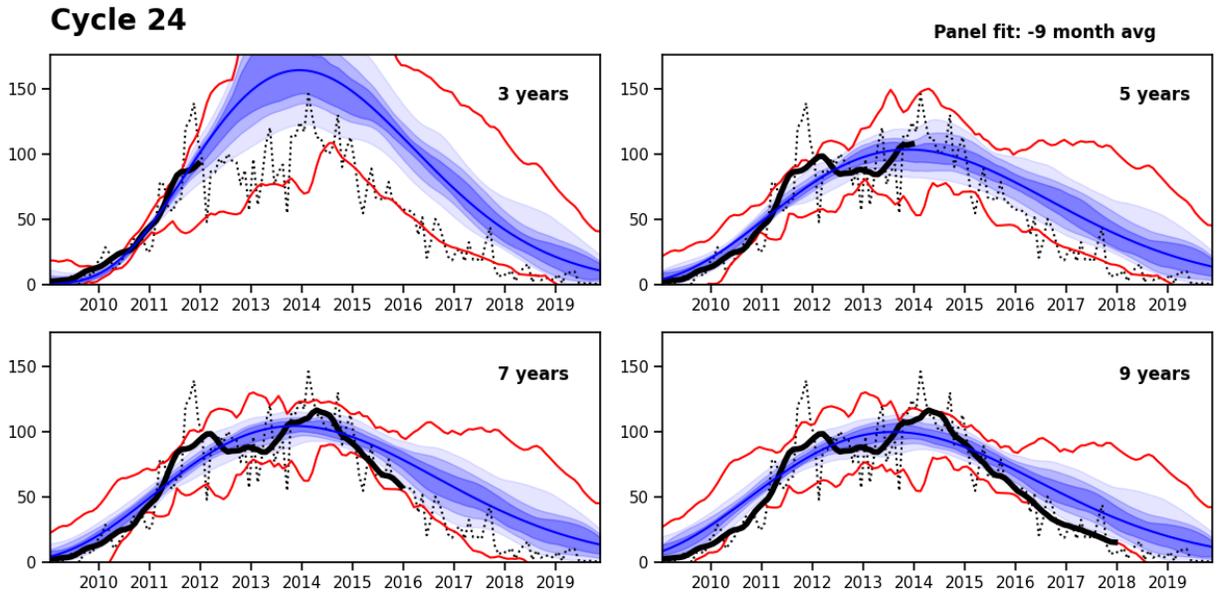
Fig. 5. As in Fig. 4 but the prediction curve is obtained by averaging two prediction months, as described in the text, separated by nine months.

profile [6]. So, we exclude these cycles from our analysis, focusing only on Cycles 6 - 24 (spanning the years 1811 - 2019). So, this is an empirical prediction method based on 200 years of sunspot data.

For each time and prediction time, quartiles are computed based on the residuals computed for the 19 viable cycles. Overprediction is not necessarily symmetric with underprediction so we handle the positive and negative residuals separately. The 25%, 50%, and 75% quartiles are shown in Figure 2 as shaded regions of uncertainty. Furthermore, the 50% (median) quartiles are used to provide the min and max uncertainty values in the accompanying json file (Section 1. The residual quartiles for all prediction times (in monthly intervals) are stored in a NetCDF file so the appropriate residual for a given prediction time can be accessed at any point in the cycle, as the prediction is continually updated every month.

So, each quartile is defined by an upper and lower curve that delineate the shaded regions in Figure 2. For example, the lower curve for the median (50%) quartile is the median overprediction of all viable cycles while the upper curve is the median underprediction. In order to improve the display, the upper and lower curves for the 25%, 50% and 75% quartiles shown in Figures 2, 4, and 5 have been smoothed using a Savitzky-Golay filter with a window length of 21 months and a polynomial order of 3. However, in order to highlight the full range of the residuals, smoothing has not been applied to the 100% quartiles shown by the red lines in Figures 4 and 5 (similarly for Figs. 7–24 below).

The "Predicted Max" range displayed in Figure 2 is defined by the smoothed upper and lower median (50% quartile) curves. In other words, the minimum value of the range reflects the maximum value of the lower median curve and the maximum value of the range reflects the maximum value of the upper median curve. Similarly, the time range listed for the cycle maximum is obtained by computing the minimum and maximum dates at which the lower median, upper median, and mean prediction curves peak.

We now turn to how the F10.7 cm radio flux prediction shown in the bottom frame of Figure 2 is computed. The 2019 panel computed their F10.7 flux prediction (red shaded region) by applying a fourth-order polynomial conversion function to the sunspot prediction curves. Such a correlation between sunspot number and F10.7 flux is well established and the conversion function is calibrated based on empirical measurements.

However, when we applied such a conversion function to the mean prediction for the sunspot number, we found that the curve fell well below the F10.7 radio flux observations. To produce a more accurate prediction, we first combined the sunspot number equation (above) with the polynomial conversion function into a composite fitting function for the F10.7 radio flux curve. We then used a nonlinear curve fit to fit the available F10.7 radio flux observations directly. Furthermore, we used an improved empirical calibration of the polynomial conversion function recently reported by Clette in 2021 [3] that was not available to the panel in 2019.

The empirical Clette (2021) conversion function is given by:

$$f_{10}(t) = 67.85 + 0.3845\, s(t) + 2.881 \times 10^{-3}\, s^2(t) - 7.426 \times 10^{-6}\, s^3(t) + 2.694 \times 10^{-10}\, s^4(t) \tag{4}$$

where $f_{10}(t)$ is the F10.7cm radio flux and $s(t)$ is the SSN.

Uncertainties for the F10.7 radio flux could in principle be computed in a similar manner to the procedure described above for the sunspot number. However, historical availability of F10.7 radio flux data is much more limited than the sunspot number. The Dominion Radio Astrophysical Observatory, where SWPC gets its F10.7 radio flux observations, has only been in operation since 1990 - about three solar cycles. Historical data from other locations only dates back to the mid 20th century [7]. For this reason, the quartiles for the F10.7 radio flux are computed by applying the updated polynomial conversion function to the smoothed sunspot number quartile curves. The "Predicted Max" amplitude and time ranges are computed as described above for the SSN.

## 3. VALIDATION

A. Robustness of Prediction

Since the product will be updated every month, it is important to ask how much the prediction is expected to change with each update. If the prediction were to change drastically from month to month then that would call into question its utility.

Figure 6 demonstrates that this is not the case. This shows how the prediction varies with the prediction date. The range shown for the prediction date begins two years into the cycle: Dec 2021. The curve fit method is not expected to be reliable before this point. The latest prediction shown is for November 2023, which makes use of monthly SSN data up to October 2023. This is the second prediction that was released since the experimental product was made public in October 2023.

The upper panel shows that the current mean prediction of 152 is within the range quoted for all predictions since Dec 2021. The mean prediction is as high as 184 in May 2022 but stabilizes after about three years into the cycle (Dec 2022). For the first two predictions released, the mean prediction only changed by one: from 153 to 152. So, we expect the prediction to not change substantially in the remaining months before maximum.

The situation is similar for the timing of the cycle max (lower panel). The current mean prediction of Sept 2024 is within one month of the range that has been produced by the algorithm since Dec 2021 (apart from Jan 2022 when it was

within two months). The last time the mean prediction has been other than Sept or Oct 2024 is for a prediction date of September, 2022. In the first two months since the experimental product became public, the range has tightened from Jan 2024 - March 2025 to Feb 2024 - Jan 2025.
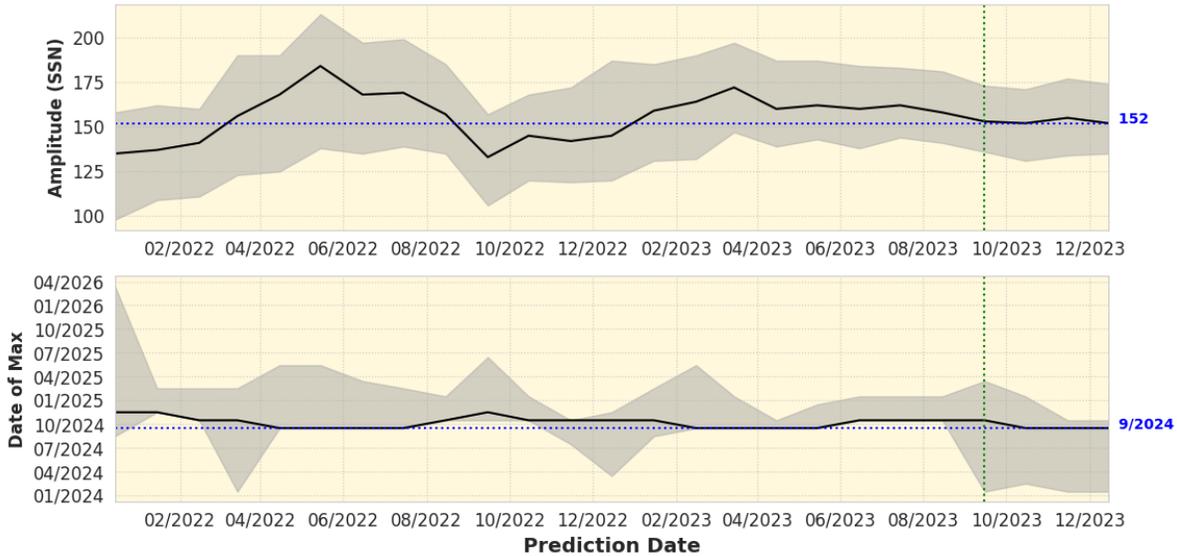
Fig. 6. The upper and lower panels demonstrate how much the amplitude and timing of the cycle prediction changes with the date of prediction (horizontal axis). The range of the prediction date extends from Dec 2021 to Jan 2024. Black lines indicate the mean prediction and shaded regions indicate the range, as given in Figure 2. Horizontal dotted blue lines indicate the latest mean prediction (labeled in blue) and vertical dotted green lines indicate the date when the experimental product was released to the public (Oct 2023).

B. Application to Previous Cycles

Figures 7–24 show the prediction method applied to cycles 6 through 23. The different curves correspond the Cycle 24 results shown in Figure 5, with similar prediction times of 3, 5, 7, and 9 years. The quartiles are computed as in Figure 2 but here, as in Figures 4 and 5, they are shown for the full range of the cycle, not just the time after the prediction time. This helps to demonstrate how accurately the curve fits and uncertainty estimates reflect the nature of the observational data.

As expected, the full range of the residual (unsmoothed 100% quartile; red lines) is largest early in the cycle, where the prediction is most uncertain. Beyond about 5 years the prediction and the associated uncertainty become fairly stable, changing little thereafter. The residual quartiles are computed as an absolute number rather than a relative number so they appear larger in smaller cycles (e.g. 6, 12) than in larger cycles (e.g. 19, 21). Near cycle maximum, the largest residuals arise from the double-peaked nature of many cycles, which is not captured by the fitting function, eq. (1). Often (though not always) this double-peaked maximum is associated with phase differences between the northern and southern hemispheres.

C. Comparison with Other Model Configurations

Comparisons between different prediction methods can be made by comparing residuals, as shown in Fig. 25. Here the shaded blue region shows the full range of the prediction residuals (100% quartile) obtained by doing a direct two-parameter fit to equation (1) with the b and c coefficients given by equations (2) and (3). We refer to this as the Panel fit because this is the same functional form as was used for the 2019 prediction curve shown in Figure 1 (red). As in Figures 4 through 24, results are shown for prediction times of 3, 5, 7, and 9 years into the cycle.

We use the same Panel fitting function and parameters for the experimental product shown in Figure 2. However, for the operational product, as discussed in Section 2, we average two prediction times in order to make the prediction more robust. In particular, we average the current prediction with the one from 9 months prior. We will refer to this as the Experimental Prediction. The residuals (100% quartile) for this Experimental Prediction are shown in Figure 25 as the red shaded region.
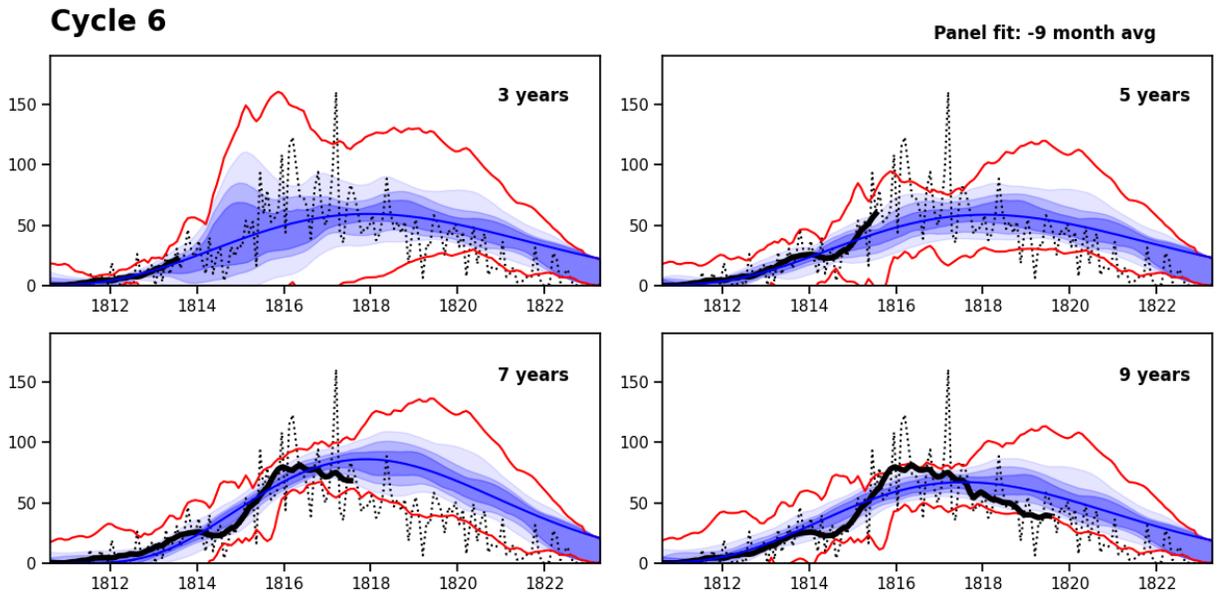
Fig. 7. As in Fig. 5 but for Cycle 6.
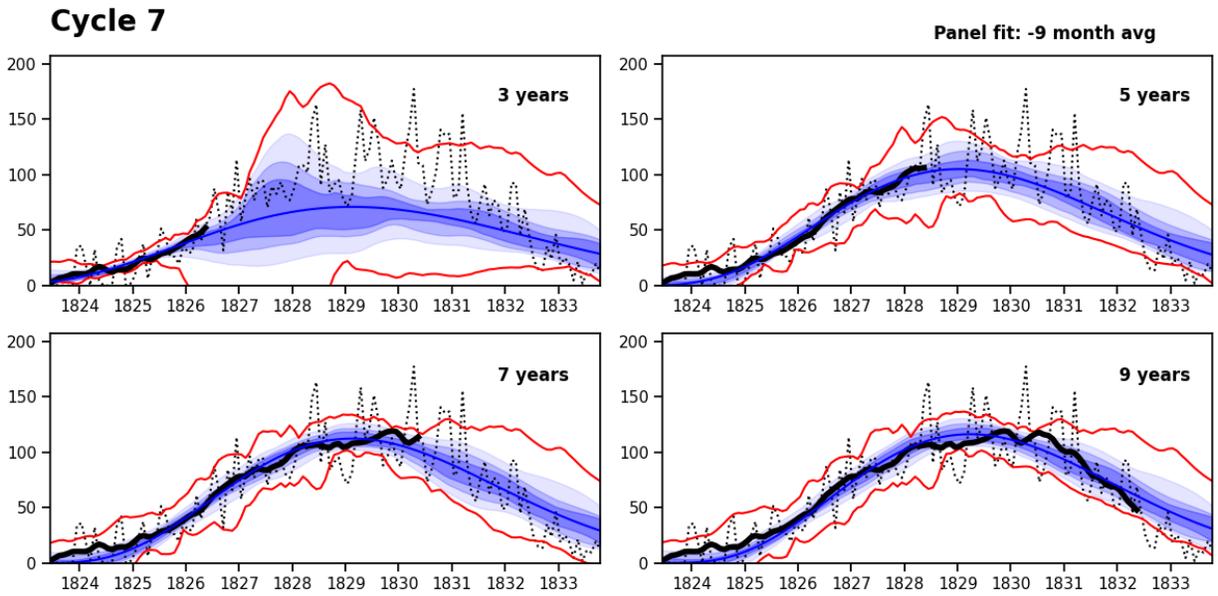
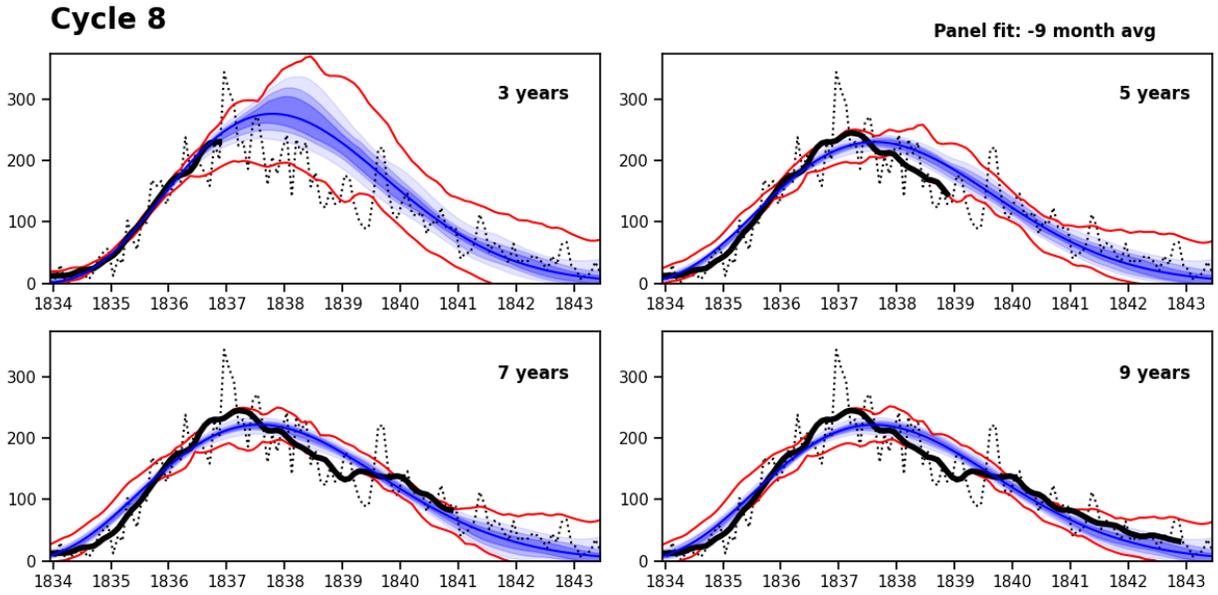**Fig. 8.** As in Fig. 5 but for Cycle 7.
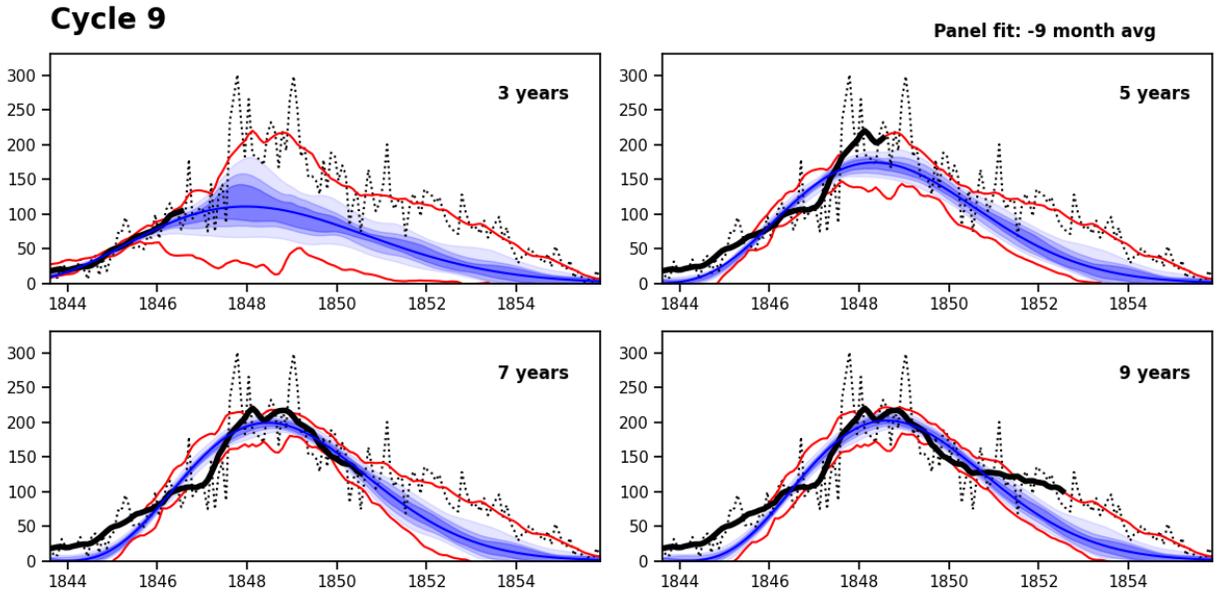
Cycle 8

Fig. 9. As in Fig. 5 but for Cycle 8.

Cycle 9

Fig. 10. As in Fig. 5 but for Cycle 9.
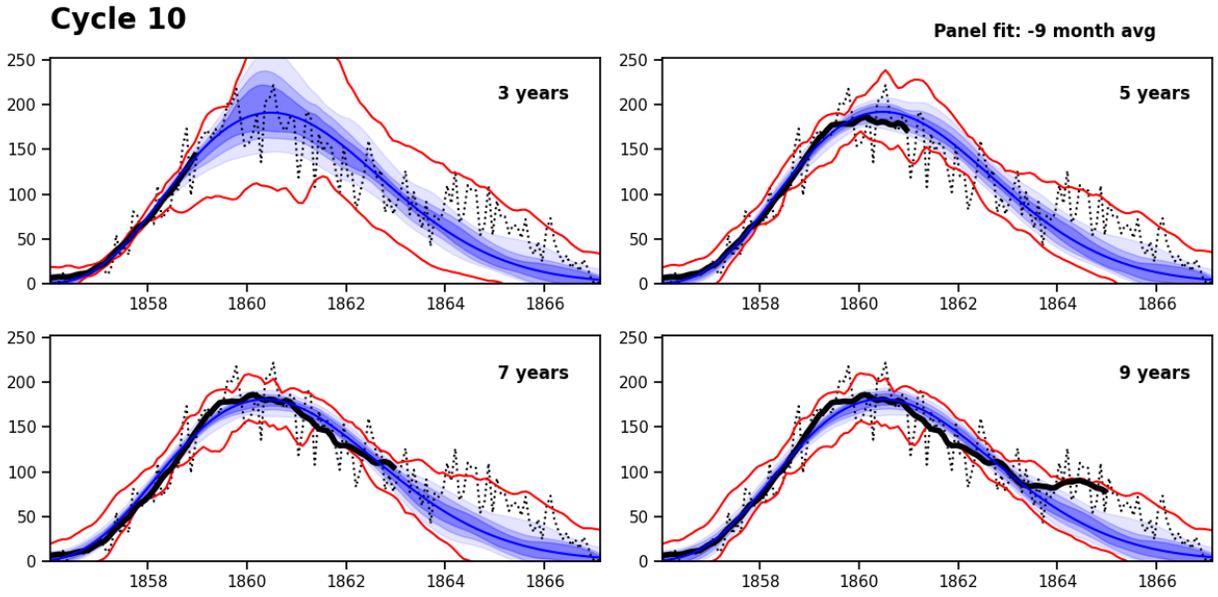
Cycle 10

Fig. 11. As in Fig. 5 but for Cycle 10.
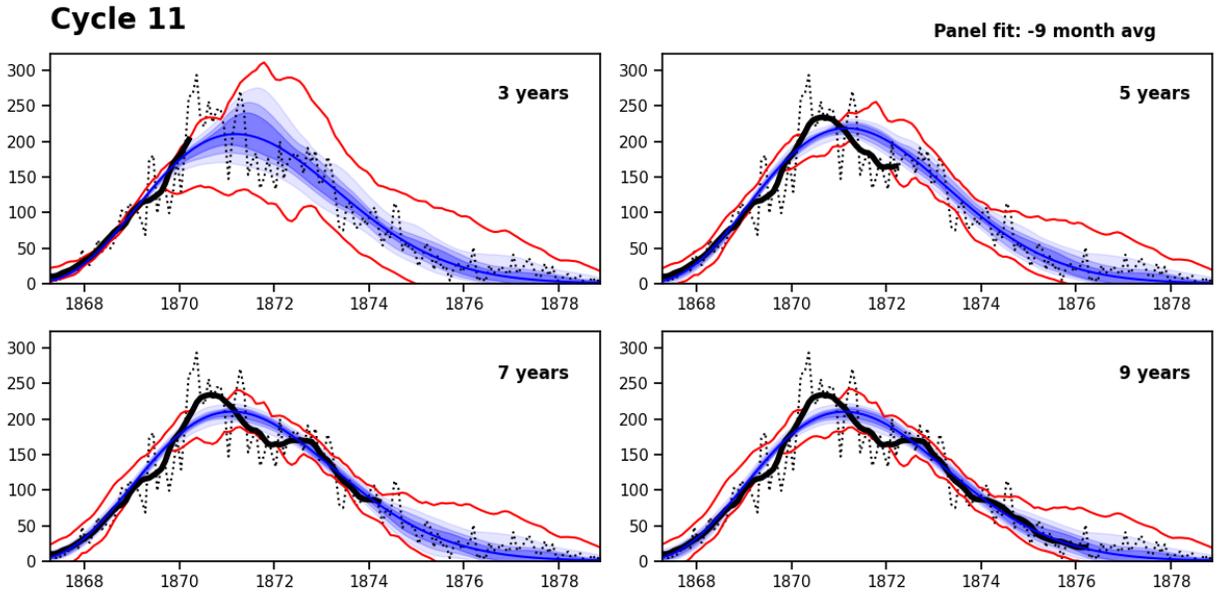
Cycle 11

Fig. 12. As in Fig. 5 but for Cycle 11.
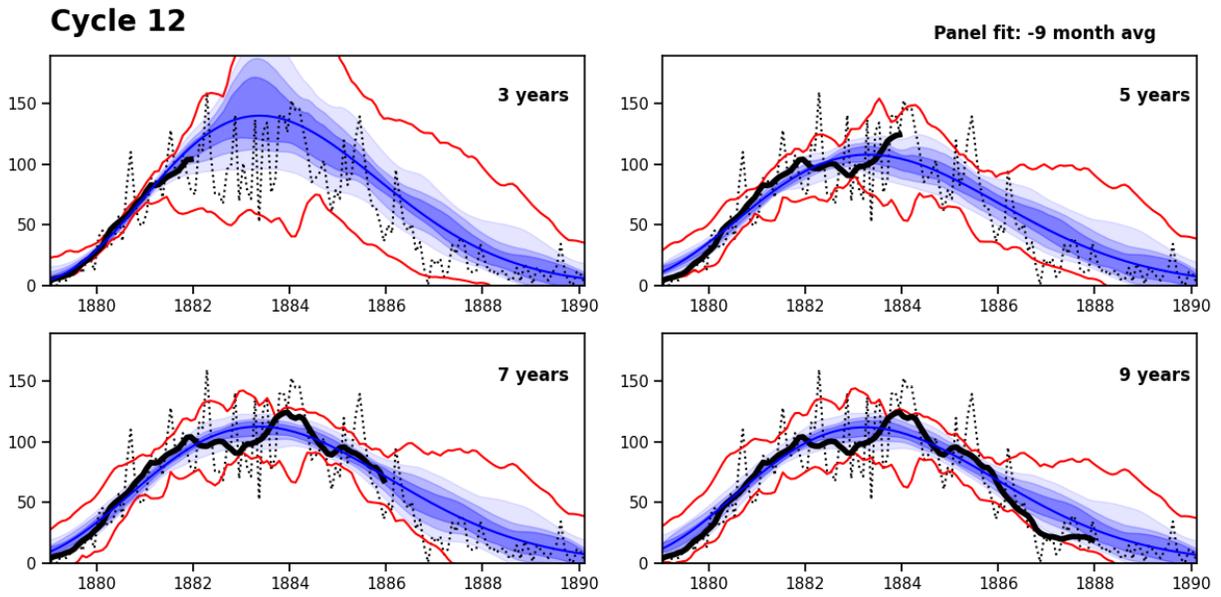
Cycle 12

Fig. 13. As in Fig. 5 but for Cycle 12.
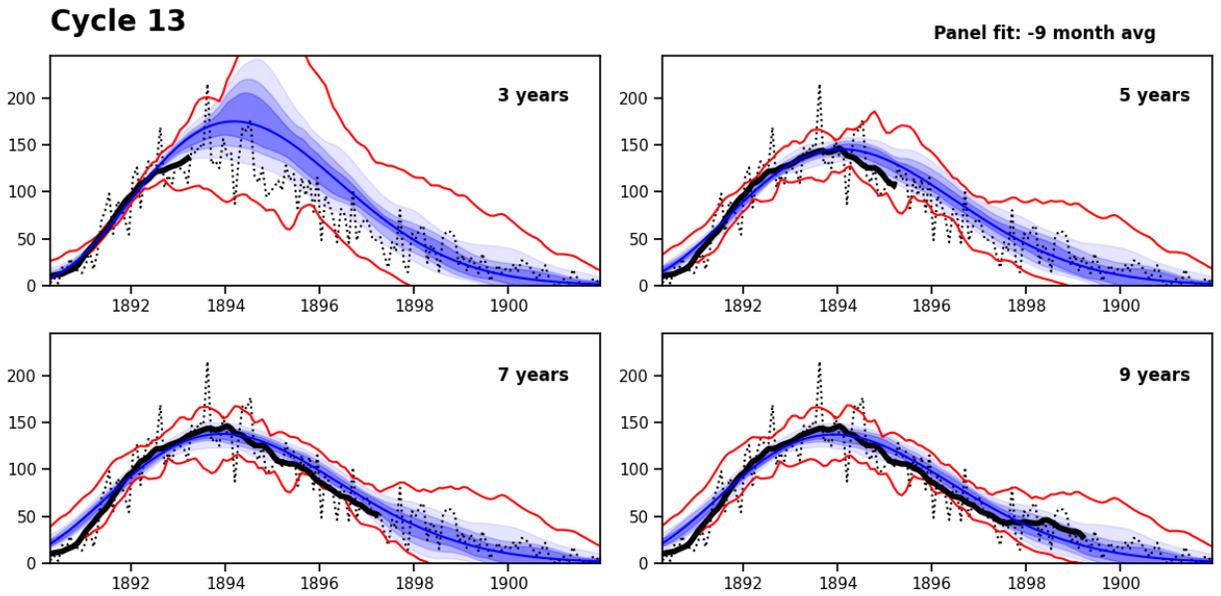
Cycle 13

Fig. 14. As in Fig. 5 but for Cycle 13.
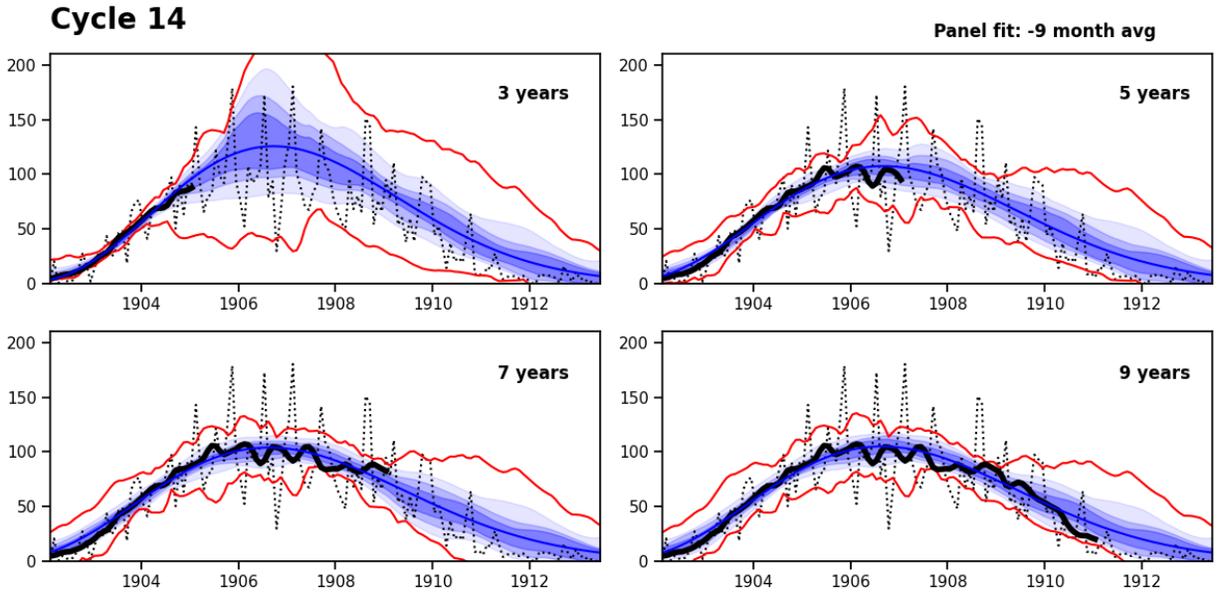
Cycle 14

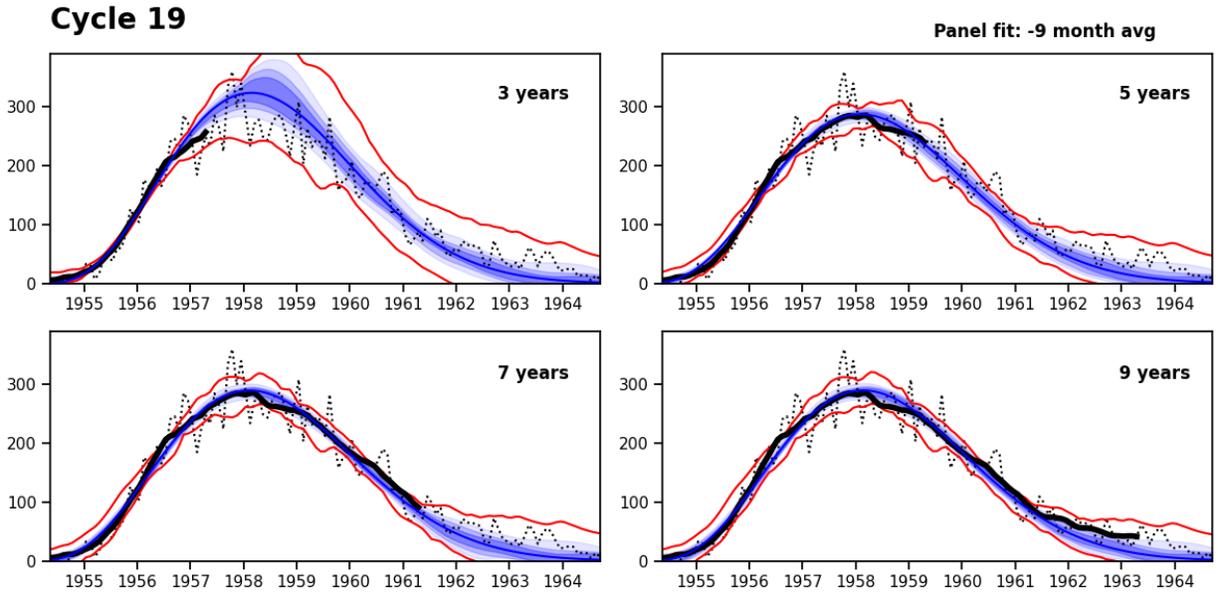**Fig. 15.** As in Fig. 5 but for Cycle 14.
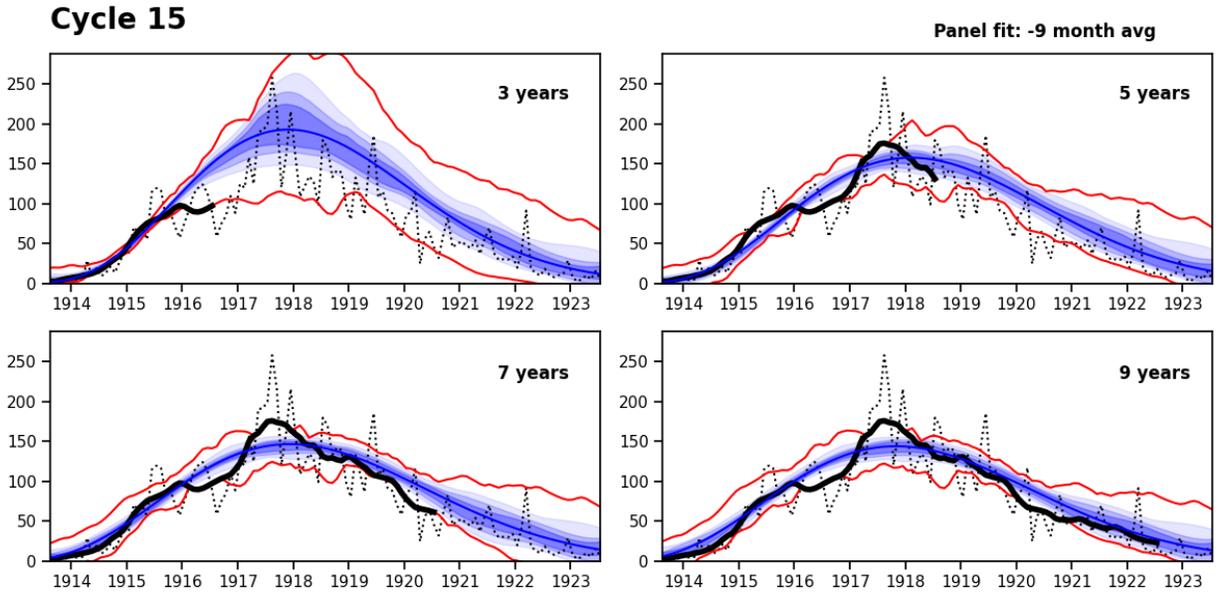
Cycle 15

Fig. 16. As in Fig. 5 but for Cycle 15.
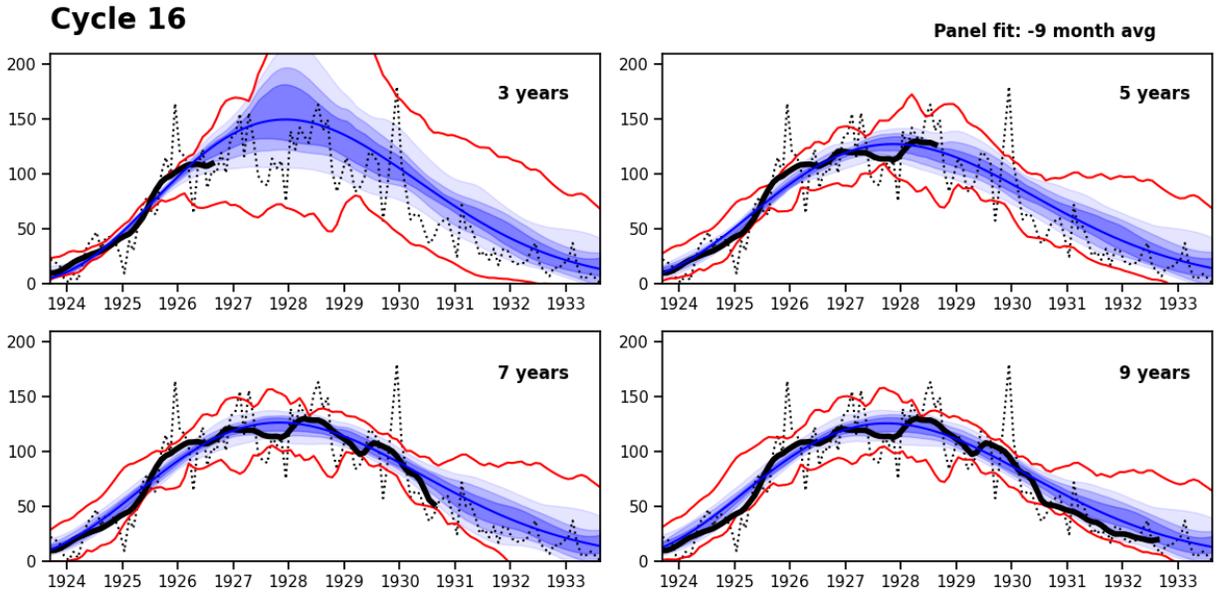
Fig. 17. As in Fig. 5 but for Cycle 16.
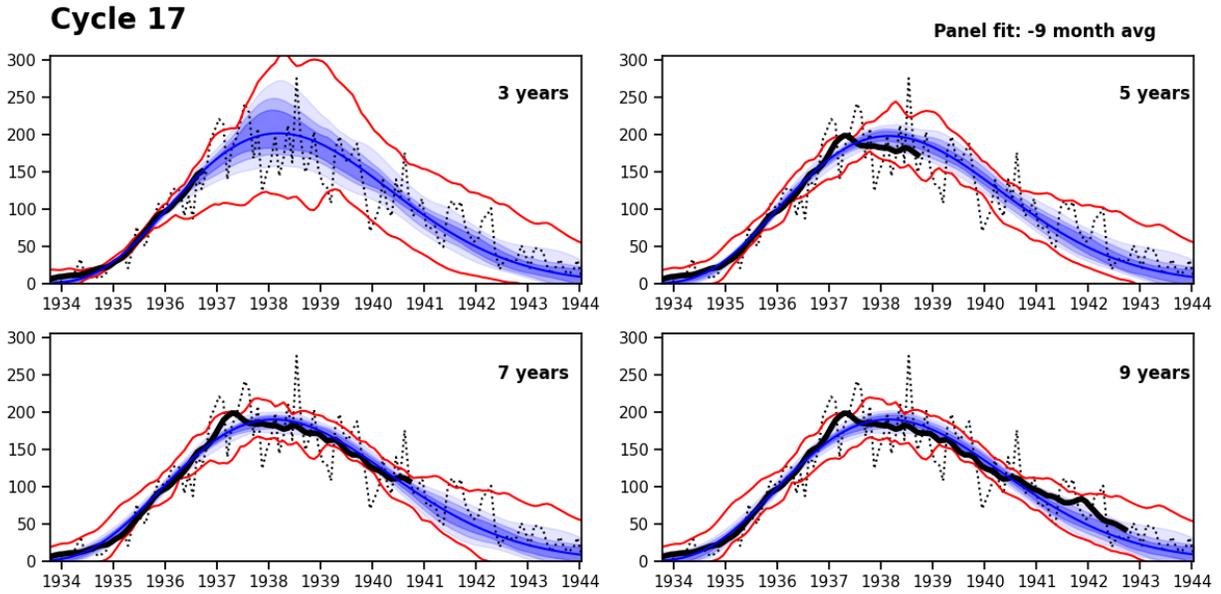
Fig. 18. As in Fig. 5 but for Cycle 17.
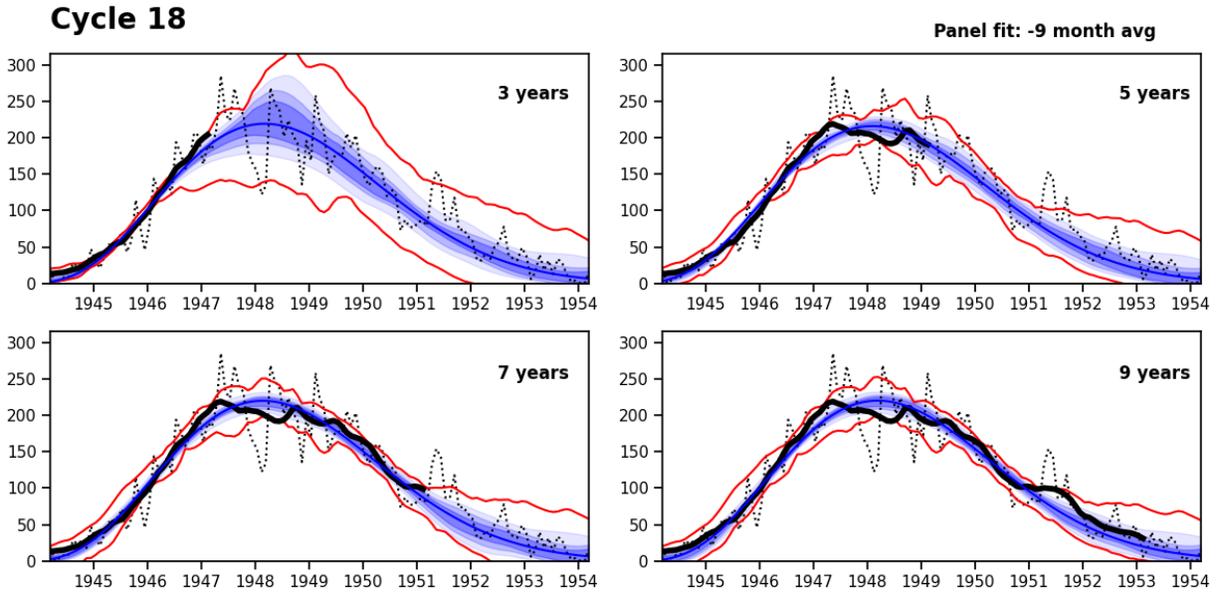
Fig. 19. As in Fig. 5 but for Cycle 18.

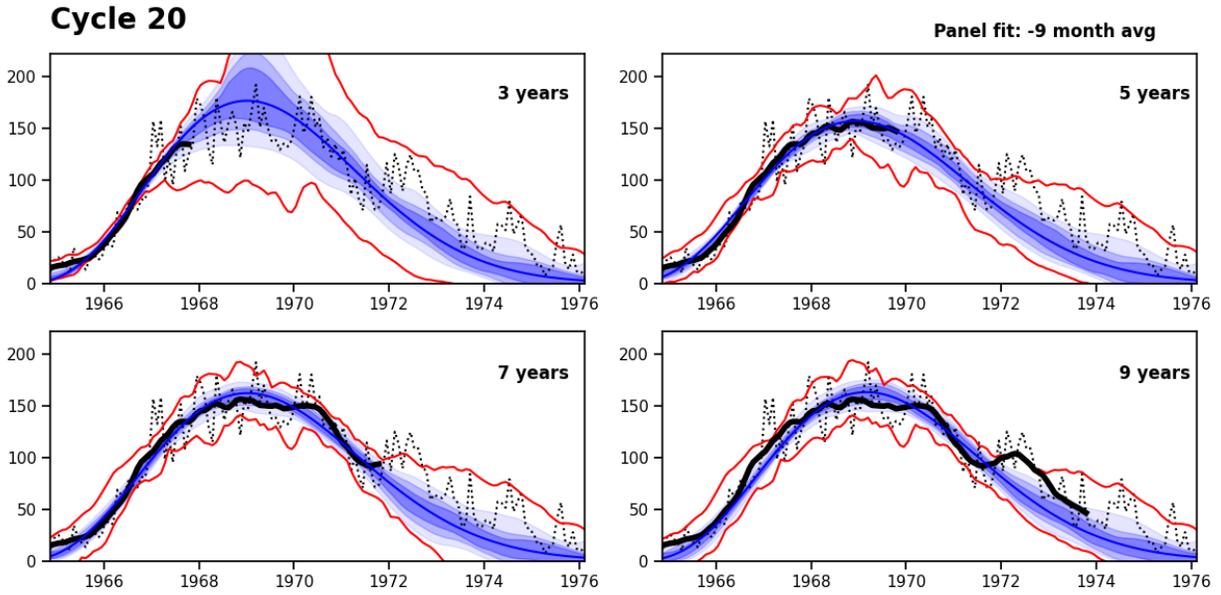**Fig. 20.** As in Fig. 5 but for Cycle 19.
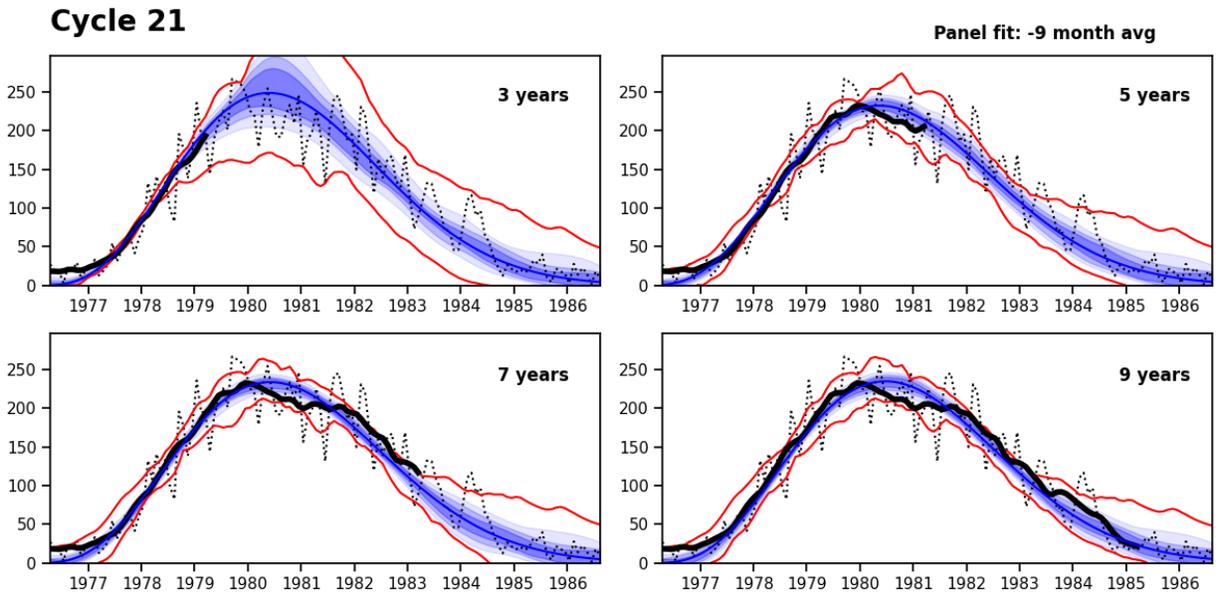
Fig. 21. As in Fig. 5 but for Cycle 20.

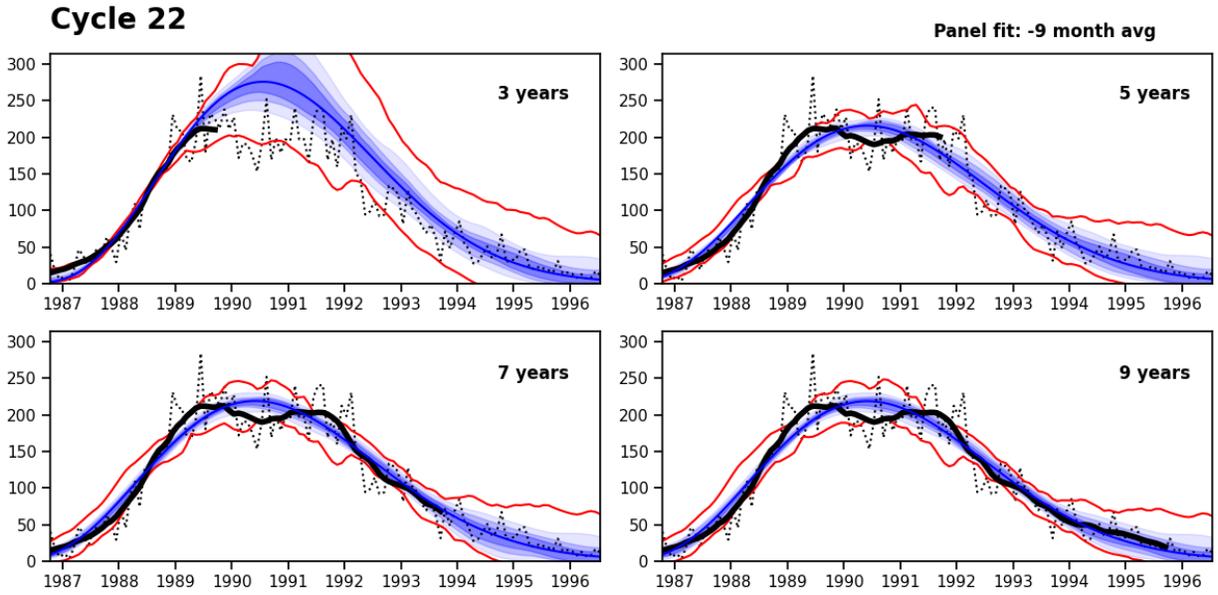**Fig. 22.** As in Fig. 5 but for Cycle 21.
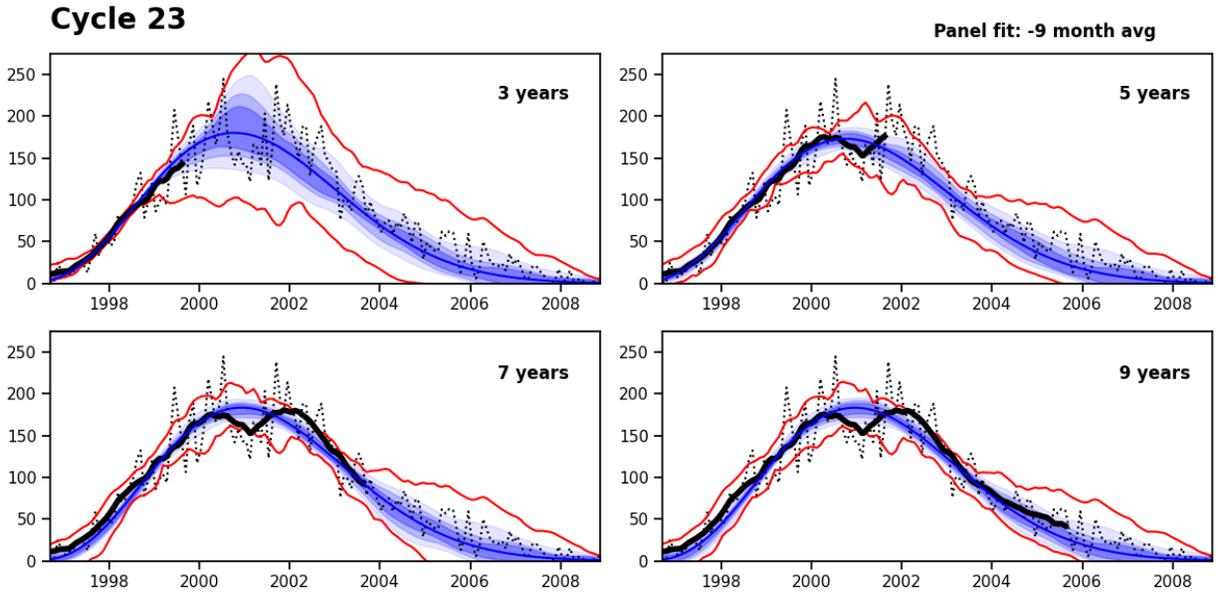
Fig. 23. As in Fig. 5 but for Cycle 22.

Fig. 24. As in Fig. 5 but for Cycle 23.

The residuals are computed by subtracting the curve fit from the observed smoothed SSN for each cycle. So, an overprediction from the curve fit would show up as a negative residual. This is clear by considering the blue curve in the upper left panel of Figure 25. Here the prediction time is 3 years. The maximum negative residual for this prediction time occurs between 4-7 years into the cycle, where it reaches a magnitude as high as -100. Since Cycle 24 had the highest negative residual of all the cycles considered at this prediction time, this corresponds to the overprediction highlighted in the upper left panel of Figure 4.

As previously noted in the dicussion of Figure 5, this overprediction is reduced in the Experimental Prediction by averaging two lead times. This is seen in the upper left panel of Figure 25 as a reduced magnitude for the negative side of the red curve at a time of 4-6 years.
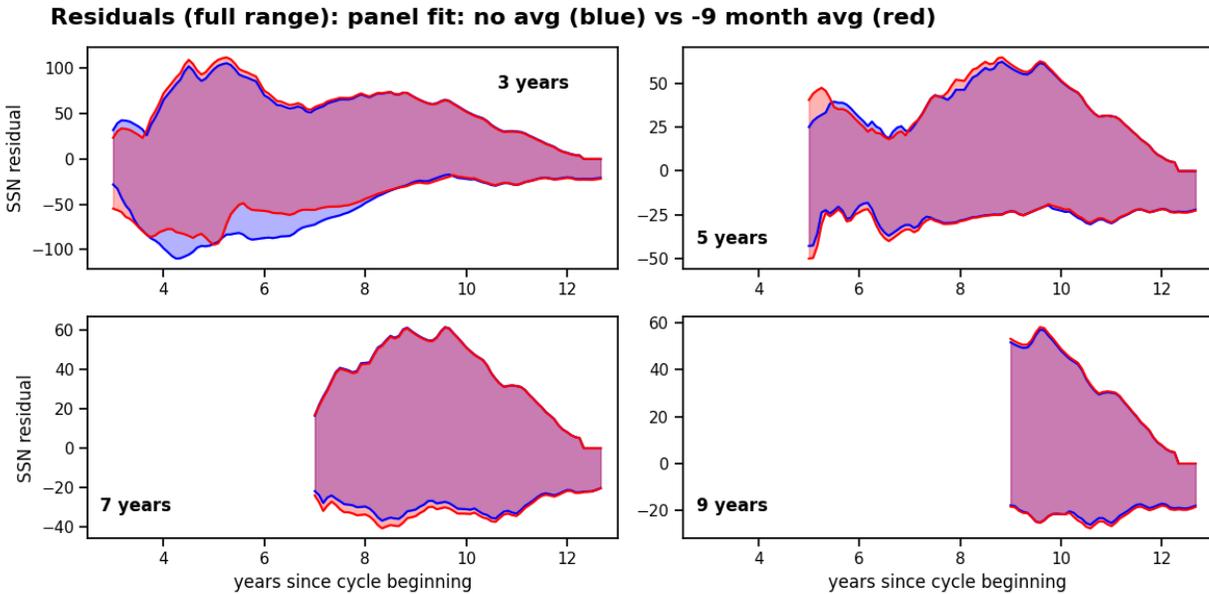
Fig. 25. The full range of the residual (100% quartile) obtained with the direct Panel fit (blue) is compared to the corresponding residual for the Experimental Prediction (red), which averages two prediction times separated by 9 months as described in the text. Different frames correspond to prediction times of 3, 5, 7, and 9 years as indicated. Residuals are shown only for the future, i.e. $t \geq t_p$

So the Experimental Prediction reduces the overprediction seen for Cycle 24, as noted in Section 2. And, it reduces the error bars as quantified by the 100% quartile, at least with regard to overprediction at a prediction time of 3 years. Elsewhere the magnitude of the prediction residuals seen in Figure 25 is similar.

However, the median residual is actually worse for the Experimental Prediction at a prediction time of 3 years, as shown in the upper left panel of Figure 26. This suggests that the direct Panel fit might be a more accurate predictor, at least for a prediction time 3 years into the cycle.

But we are already more than three years into Cycle 25, which started in December, 2019. For the remainder of the cycle, only prediction times beyond about 3.6 years are of relevance. As shown in Figure 27 (upper left), the situation reverses at this prediction time. Now the red (Experimental Prediction) gives a lower median residual than the blue (direct Panel fit), at least around 4-5 years. Elsewhere the mean residuals are similar. The implication is that, by 3.6 years, the 9-month prior prediction has become more reliable. Meanwhile, the 100% quartile (not shown) at a prediction time of 3.6 years is comparable for the Experimental Prediction and the Panel fit.
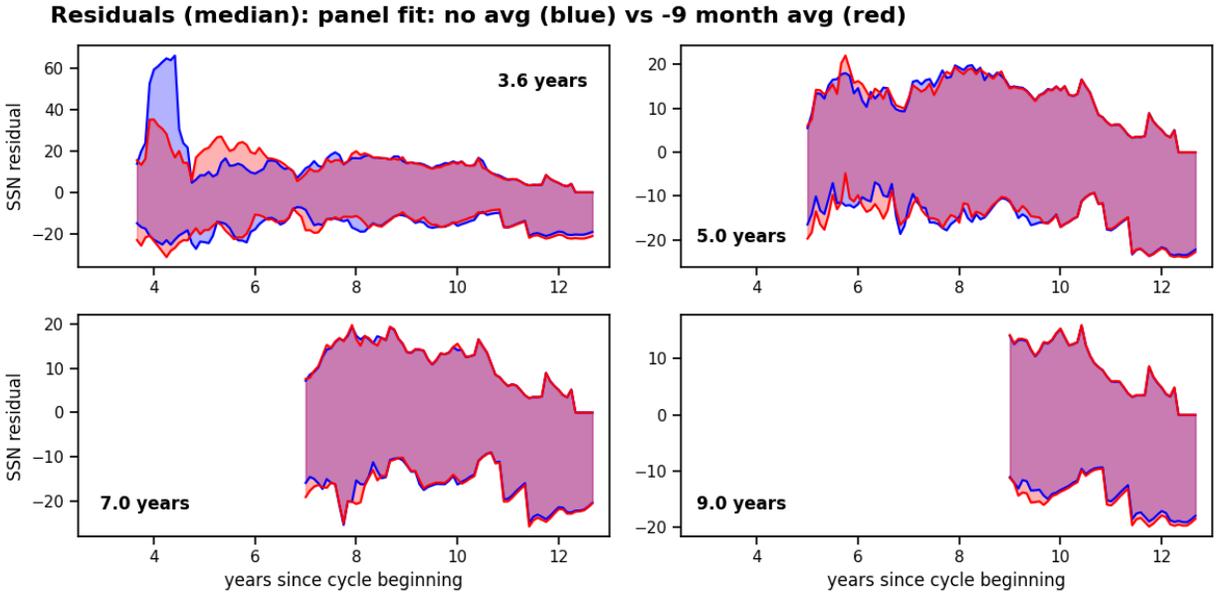
The overall performance of the Experimental Prediction and the Panel fit is similar; neither stands out as being unambiguously superior. However, given that we are already more than 3.6 years into Cycle 25, we conclude that averaging two lead times provides a somewhat more robust prediction without sacrificing accuracy. Furthermore, though the results are again somewhat ambiguous, we find that a 9-month interval between the two fits gives an optimal prediction. This is demonstrated in Figures 28 and 29.

Again, the time interval between the fits makes the most difference early in the cycle. Still, using a 6-month or a 12-month interval does not offer a clear advantage over a 9-month interval. Furthermore, a 12-month interval is slightly inferior to a 9-month interval when considering the full range of the residual (Fig. 30). For these reasons, we have chosen a 9-month interval for the Experimental Product.

Another variation on our curve fit prediction method has recently been proposed by Upton & Hathaway [9]. This uses

Residuals (median): panel fit: no avg (blue) vs -9 month avg (red)
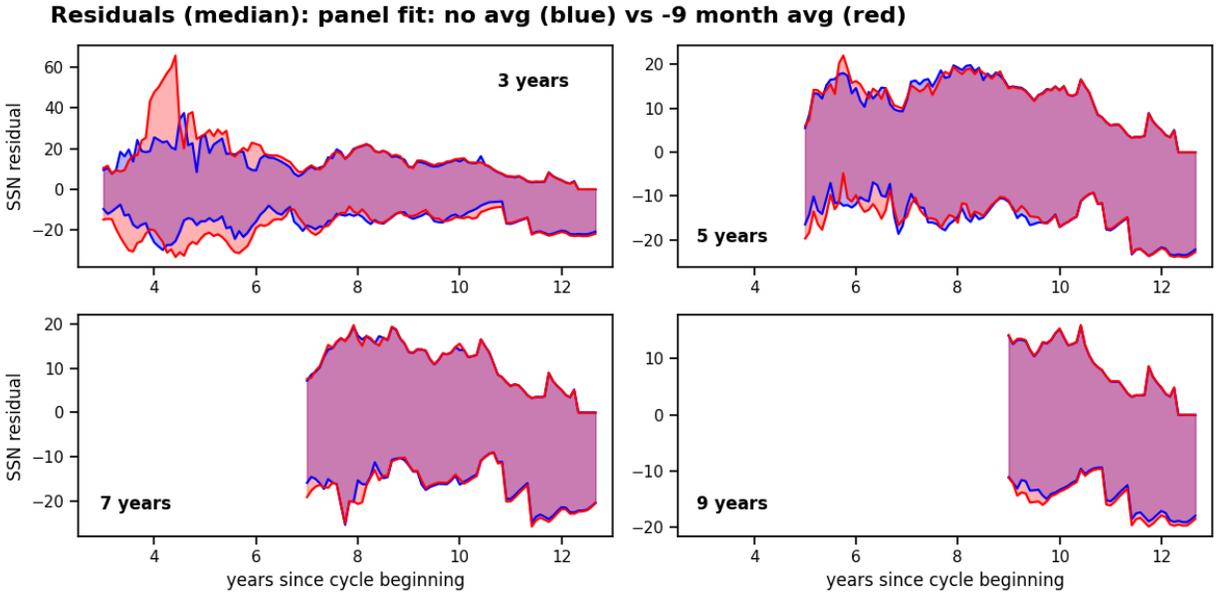
Fig. 26. As in Figure 25 but for the median residual (50% quartile).

Residuals (median): panel fit: no avg (blue) vs -9 month avg (red)

Fig. 27. As in Figure 26 but with the 3-year prediction time in the upper left replaced by a 3.6-year prediction time.

19

Residuals (median): panel fit: -6 (blue) vs -9 month (red) avg
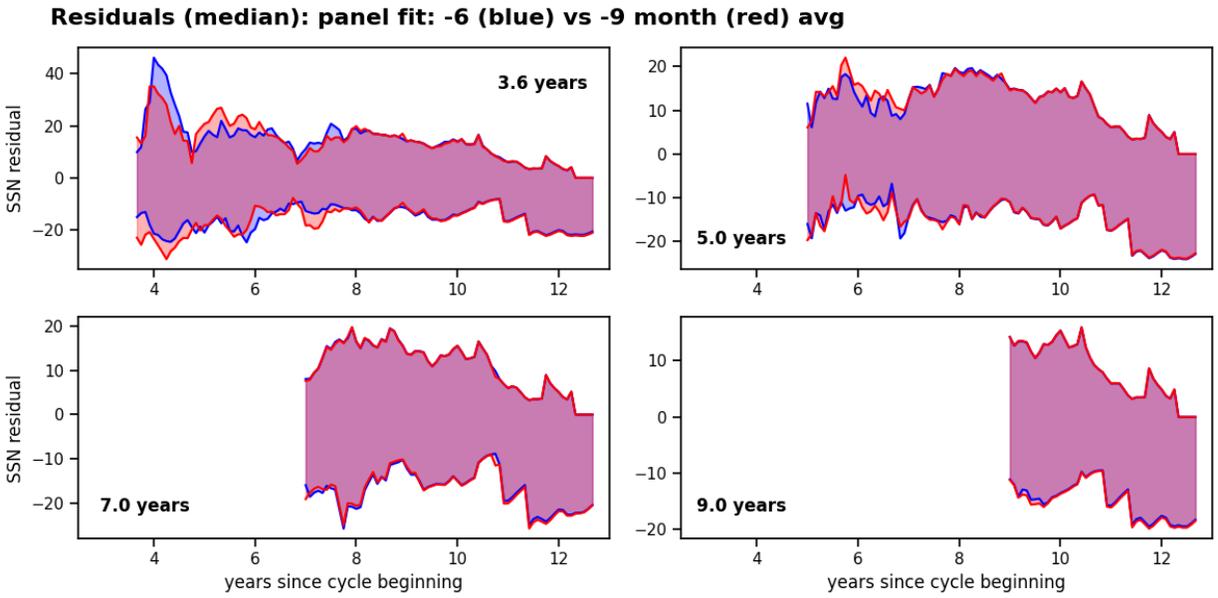
Fig. 28. As in Figure 27 but comparing the Experimental Prediction (red) to a 6-month interval between the two averaged fits (blue), rather than 9 months.

Residuals (median): panel fit: -12 (blue) vs -9 month (red) avg
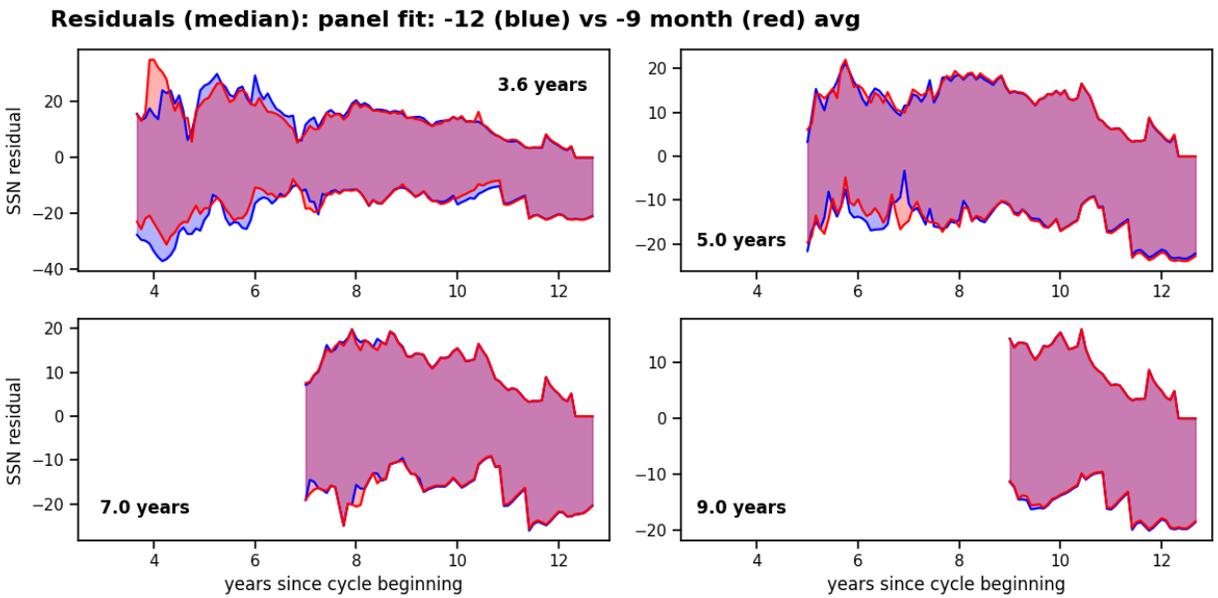
Fig. 29. As in Figure 28 but comparing the Experimental Prediction (red) to a 12-month interval between the two averaged fits.
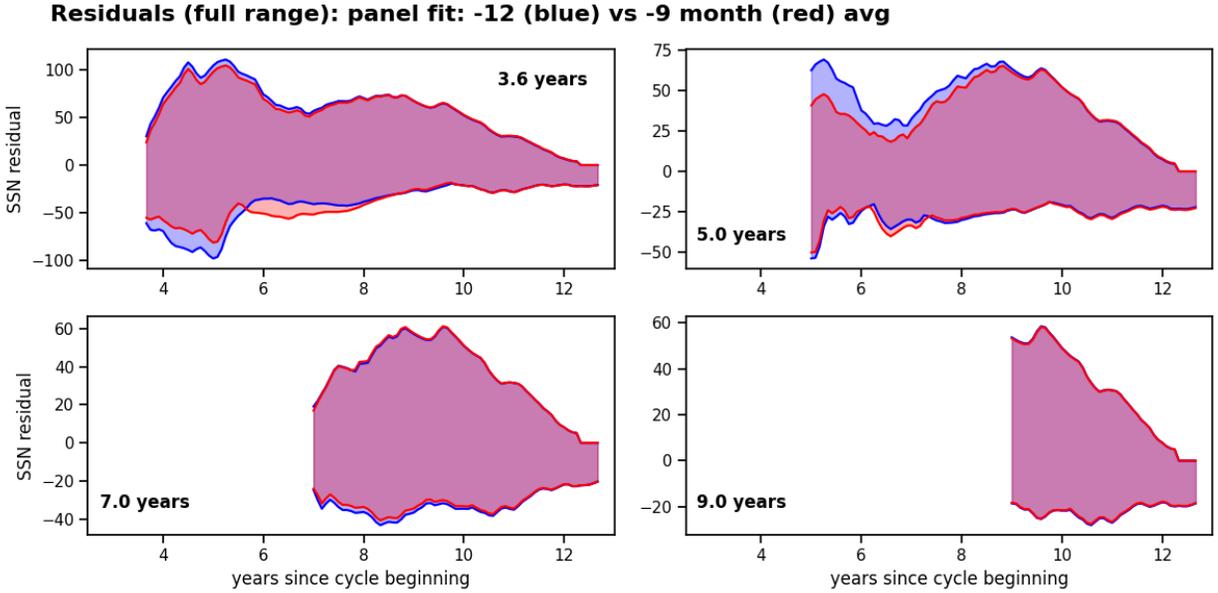
Fig. 30. As in Figure 29 but for the full range of the residual (100% quartile).

the same functional form as in equation (1) but a different parameterization for b and c:

$$b = 36.3 + 0.72A^{-1/2} \tag{5}$$

$$c = 0.70 \quad . \tag{6}$$

We refer to a curve-fit prediction made using this parameterization as UH23. Figures 31 and 32 compare the residuals obtained with the UH23 parameterization (red) to our Experimental Prediction (blue). For this comparison, we averaged two UH23 fits separated by an interval of 9 months as described above for the Experimental Prediction.

We find the Experimental Prediction to give better performance throughout, except possibly for the median residual at a prediction time of 7 years. However, 7 years is typically after cycle maximum so this improved performance alone is not compelling enough to adopt this approach. The discrepancy is particularly apparent late in the cycle, where we find the UH23 parameterization tends to overpredict.

Adopting the same parameterization used by the 2019 Panel has the added advantage that it can be related more easily to the 2019 Panel prediction shown as the red shaded region on the updated product, Figure 2. In other words, the red shaded region and the magenta curve use the same functional representation for the cycle curve; the amplitude and start time are merely recalibrated to available observations (and averaged among two prediction times).

For these reasons, we have adopted the panel parameterization described in Section 2 in our Experimental Prediction.

### D. Comparison to Alternative Prediction Approaches

As another reference point for validation, we can compare the prediction presented in the new product to other recent predictions for Solar Cycle 25 that make use of the latest observational data. One such prediction, updated in 2023 from earlier predictions made by the same group, was recently published by McIntosh et al. [5]. This predicts a peak sunspot number of 184 +/- 17 to occur between late 2023 and mid 2024. This is based on closely following the equatorward migration and temporal phasing of observed features on the solar surface including EUV bright points and magnetic active regions.

Meanwhile, Upton & Hathaway [9] predict a maximum SSN of 134 ± 8, to occur in fall 2024. This is based in part on a curve fit similar to that presented here, but it uses different parameterizations for b and c in eq. (1), and it does not average multiple lead times. Furthermore, Upton & Hathaway 2023 also take into account geomagnetic precursors in coming up with their amplitude prediction.

Another prediction comes from NASA Marshall Space Flight Center, which is updated monthly. As of October, 2023, they predict a peak amplitude of 137 in summer 2024 with a wide uncertainty ranging from 116 to 210 (late 2023 to late 2024). An amplitude "only slightly larger than Cycle 24 [115]" is also predicted by Mursula [7] who attributes cycle variations to the interaction of the cyclic dynamo-generated field with a tilted, relic magnetic field in the deep radiative interior of the Sun, inferred from north-south asymmetries in the F10.7 radio flux and SSN.
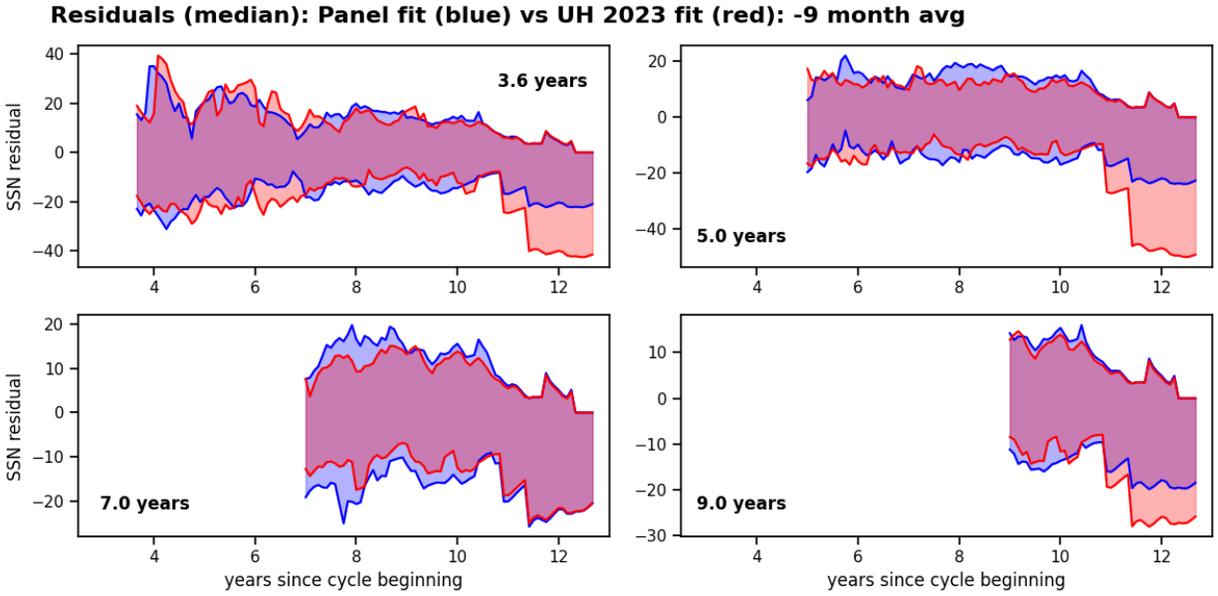
Fig. 31. Similar to Figure 27 but comparing the Experimental Prediction (blue) to the UH23 fit (obtained, like the Experimental Prediction, by averaging two lead times separated by 9 months). This is for the median residual (50% quartile).
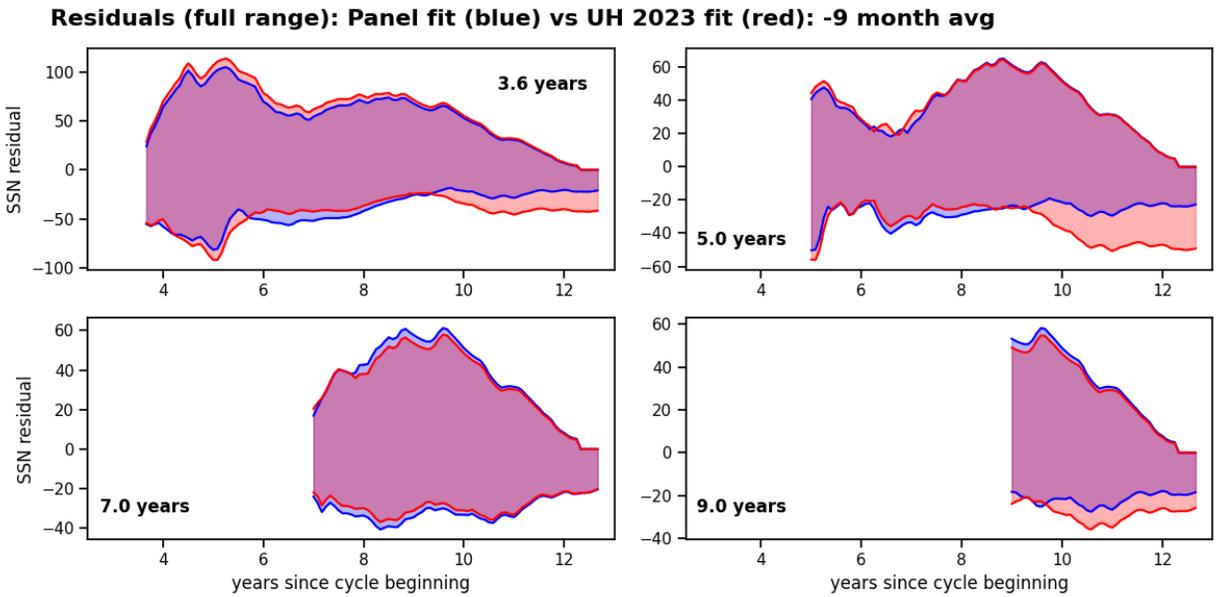
Fig. 32. Similar to Figure 31 but for the full range of the residual (100% quartile).

The Solar Influences Data analysis Center (SIDC) provides a medium-term (12-month) SSN prediction, updated monthly, based on the statistics of past SSN observations, geomagnetic precursors, and the assimilation of new data by means of a Kalman filter [8]. As of October, 2023, this predicts a peak SSN before October 2024 between 140 and 185.

As shown in Figure 2, our new product is comparable to these other predictions. As of October, 2023, the predicted peak amplitude is 137 - 173 (mean 154) occurring in January-October 2024. This places it somewhat higher that Upton & Hathaway but somewhat lower than McIntosh et al.

REFERENCES

1. F. Clette, L. Svalgaard, J.M. Vaquero & E.W. Cliver 2014, "Revisiting the Sunspot Number", Space Science Reviews, **186** (1-4), 35–103, DOI: 10.1007/s11214-014-0074-2
2. F. Clette & L. Lefèvre 2016, "The New Sunspot Number: Assembling All Corrections", Solar Physics, **291**, DOI: 10.1007/s11207-016-1014-y
3. F. Clette 2021, "Is the F10.7 cm – Sunspot Number Relation Linear and Stable?", J. Space Weather Space Clim., **11**, 2, https://doi.org/10.1051/swsc/2020071
4. D.H. Hathaway, R.M. Wilson, & E.J. Reichmann 1994, "The Shape of the Sunspot Cycle", Solar Physics, **151**: 177–190
5. S.W. McIntosh, R.J. Leamon, & R. Egeland 2023, "Deciphering Solar Magnetic Activity: The (Solar) Hale Cycle Terminator of 2021" Front. Astron. Space Sci., 10:1050523, doi: 10.3389/fspas.2023.1050523
6. A. Muñoz-Jaramillo & J.M. Vaquero 2019, "Visualization of the Challenges and Limitations of the Long-Term Sunspot Record", Nature Astronomy, **3**, 205-211, https://doi.org/10.1038/s41550-018-0638-2
7. K. Mursula 2023, "Hale Cycle in Solar Hemispheric Radio Flux and Sunspots: Evidence for a Northward-Shifted Relic Field", Astronomy & Astrophysics, **674**, A182, https://doi.org/10.1051/0004-6361/202345999
8. T. Podladchikova & R. Van der Linden, 2012, "A Kalman Filter Technique for Improving Medium-Term Predictions of the Sunspot Number", Solar Physics, **277**, 397–416.
9. L. Upton & D.H. Hathaway 2023, "Solar Cycle Precursors and the Outlook for Solar Cycle 25", J. Geophys. Res. Space Physics, **128**, https://doi.org/10.1029/2023JA031681